Aggregation and electronically induced migration of oxygen vacancies in TiO_2 anatase

Martin Setvin, Michael Schmid, and Ulrike Diebold
Institute of Applied Physics, Vienna University of Technology, Wiedner Hauptstrasse 8-10/134, 1040 Vienna, Austria
(Received 2 March 2015; published 6 May 2015)

The influence of the electric field and electric current on the behavior of oxygen vacancies (V_Os) in TiO_2 anatase was investigated with scanning tunneling microscopy (STM). At the anatase (101) surface V_Os are not stable; they migrate into the bulk at temperatures above 200 K. Scanning a clean anatase (101) surface at a sample bias greater than $\approx+4.3$ V results in surface V_Os in the scanned area, suggesting that subsurface V_Os migrate back to the surface. To test this hypothesis, surface V_Os were first created through bombardment with energetic electrons. The sample was then mildly annealed, which caused the V_Os to move to the subsurface region, where they formed vacancy clusters. These V_O clusters have various, distinct shapes. Scanning V_O clusters with a high STM bias reproducibly converts them back into groupings of surface V_O, with a configuration that is characteristic for each type of cluster. The dependence of the subsurface-to-surface V_O migration on the applied STM bias voltage, tunneling current, and sample temperature was investigated systematically. The results point towards a key role of energetic, "hot" electrons in this process. The findings are closely related to the memristive behavior of oxides and oxygen diffusion in solid-oxide membranes.

DOI: 10.1103/PhysRevB.91.195403 PACS number(s): 68.47.Gh, 82.47.Ed, 73.20.At

I. INTRODUCTION

The influence of electric fields on the behavior of oxygen vacancies (V_Os) in metal oxides is of key importance for several applications of these materials. For example, the memristive switching in oxides is a promising approach for data storing [1–4]. While it is clear that field-induced redox reactions and field-induced material migration play a key role [4], very little is known about the detailed physical mechanisms and processes occurring at atomic scale [5,6]. Similar phenomena are also essential in solid-oxide fuel cells [7,8], where oxygen is transported from the cathode to the anode through the lattice of the oxide electrolyte (typically ZrO_2 or CeO_2) via migration of oxygen vacancies.

Anatase is a metastable form of the prototypical metal oxide TiO_2 [9], a material that has been central in oxide research for decades. TiO_2 anatase is used in catalysis [10], photocatalysis [11,12], and dye-sensitized solar cells [13]. Owing to its promising electronical properties, it is also frequently investigated as a memristive material [3,4] and as a transparent conductive oxide [14].

Recently it was found that the anatase (101) surface does not contain any surface V_Os when prepared under ultrahigh vacuum (UHV) conditions by a standard sputter-annealing procedure [15]. Surface V_Os could be produced nonthermally by bombarding the sample with energetic electrons. These V_Os proved unstable and diffused to the subsurface region at temperatures as low as 200 K [16]. In our previous work [17] we have created the same atomic-size features by scanning a clean anatase (101) surface at a high sample bias of $\approx+5$ V. We concluded that these were V_Os that most likely originated from electronically induced migration of oxygen vacancies from the subsurface region to the surface.

In this work we investigate these phenomena in detail. The paper is divided into three main parts. In Sec. III A we confirm that scanning a clean anatase (101) surface at high positive sample biases creates surface V_Os. In Sec. III B we verify that the V_Os appearing on the surface indeed stem from the subsurface region. To this end we performed the following experiment: First, surface V_Os were created by electron bombardment of a defect-free surface. Then the sample was annealed above room temperature. This resulted in the migration of V_Os to the subsurface region, where they formed V_O clusters. Scanning at high bias voltage reproducibly converted these clusters back into a collection of single surface V_Os. This is a strong indication that the surface V_Os form due to migration of material between the subsurface region and the surface and are not newly created by the tip of the scanning tunneling microscope (STM). We also discuss the ramifications of the subsurface V_O clustering for surface reactivity. In Sec. III C we systematically investigate how the rate of V_O creation depends on various parameters (bias voltage U_S, tunneling current I_T, temperature, and number of scans), and determine the role of the electric field E. Based on a quantitative analysis of the experimental results, we conclude that the V_O migration occurs close to the field-emission regime in STM, and it depends on E only weakly under the experimental conditions used in this work. In Sec. III D we discuss the possible physical mechanisms underlying the STM-induced V_O migration. We identify the mechanism as a one-electron process involving hot electrons. The implications of our results for memristor research are discussed.

II. EXPERIMENTAL DETAILS

The experiments were performed in a UHV chamber at a base pressure below 1×10^{-9} Pa, equipped with a commercial Omicron LT-STM head. STM measurements were performed at $T = 78$ K or $T = 6$ K. Electrochemically etched W STM tips were cleaned by Ar^+ sputtering and treated on a Au (110) surface to obtain a reproducible, metallic tip condition. An anatase mineral sample was cleaved [18] and cleaned *in situ* by cycles of Ar^+ sputtering and annealing [19]. In a trace analysis [17], the highest level of impurity in the sample was determined as 1.1 at. % Nb.

Sample annealing was performed in a manipulator located in an adjacent preparation chamber (base pressure 3×10^{-9} Pa). The temperature was measured with a K-type

thermocouple at the heating/annealing stage. We estimate that the quoted temperatures are accurate within ±10 K. To create surface V_Os, the sample was cooled to 105 K and irradiated with electrons from a thoroughly outgassed, rastered electron gun (500 eV, current density 8 μA cm^{-2}).

III. RESULTS AND DISCUSSION

A. STM-induced surface O vacancies

Figure 1 shows the effect of scanning a clean anatase (101) surface with STM at a high positive sample bias. Single V_Os appear within the scanned area (and, depending on the tip shape, the surrounding few nanometers; see Ref. [17]). Figure 1(a) displays the as-prepared, clean anatase (101) surface; the STM image was taken with standard (low-bias) conditions. Brighter regions correspond to positions of subsurface donors [20], likely extrinsic dopants. Figure 1(b) shows the same area, but this time it is scanned at a high sample bias $U_S = +5.2$ V and a tunneling current $I_T = 0.1$ nA. Horizontal streaks indicate structural changes that occurred during the high-voltage scan (marked by arrows). The same area is imaged again in Fig. 1(c) with normal imaging conditions [after two high-bias scans such as the one in (b)]. Several new features have appeared in the area; some are marked by arrows. By comparison with e-beam-induced defects [16,17] (see also Fig. 2 below) these are identified as surface V_Os. When the same area is scanned multiple times at the same elevated bias, more oxygen vacancies are created. This is illustrated in Fig. 1(d), which shows the same area after 32 high-bias scans at the tunneling parameters of Fig. 1(b). For better orientation, the positions of the vacancies created in (b) are marked. It is rare that the V_Os move laterally by one position during a high-bias scan. We were not able to remove the V_Os with the STM tip, for example by applying a negative U_S.

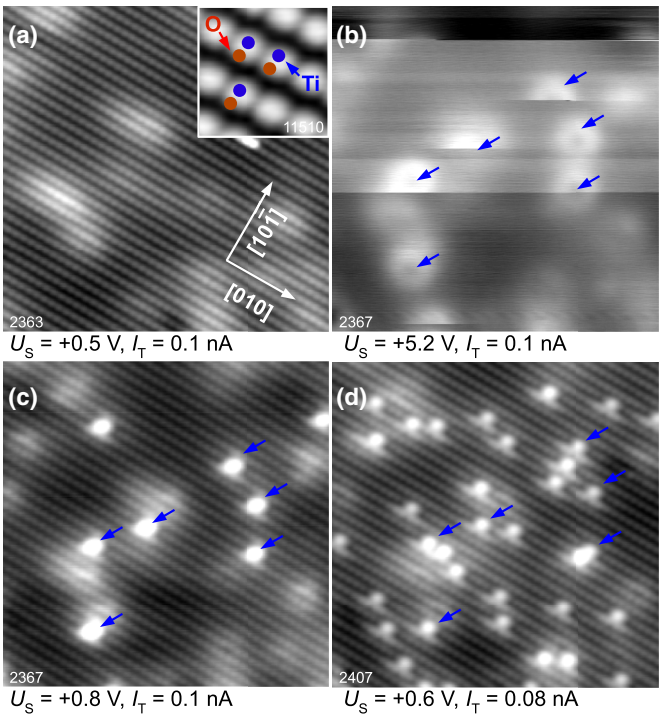

FIG. 1. (Color online) (a)–(d) Consecutive STM images (15 × 15 nm^2, $T = 6$ K) taken at the same area of an anatase (101) surface. (a) Clean surface. The inset shows a detailed STM image where the positions of surface five-coordinated Ti and two-coordinated O atoms are marked. (b) STM image taken with a high bias ($U_{Sample} = +5.2$ V). (c) Low-bias scan of the same area. Surface V_Os that appeared during the high-bias scan are marked by blue arrows. (d) Low-bias STM image after 32 high-bias scans with conditions as in (b). The arrows point to the same V_Os as in (c).

B. Formation and dissociation of V_O clusters

1. *Subsurface vacancy clusters formed by aggregation*

The surface V_Os shown in the previous section could, in principle, be generated in two different ways: either by desorbing two-coordinated surface O_{2c} atoms (e.g., via electron or field-induced desorption), or by "pulling" subsurface V_Os to the surface. (More precisely, by pushing surface oxygen atoms deeper into the lattice.) Several previous observations point towards the second possibility. First, the threshold for electron-induced desorption is in the range of tens of eV [21], much higher than what can be achieved in STM. Second, the tip is at a negative potential with respect to the sample, thus it should repel rather than attract the O anions. Third, on TiO_2 rutile (110) it was shown that the STM tip can move V_Os laterally [22], so a vertical motion of V_Os is not inconceivable. Nevertheless, we designed an experiment to test whether it is indeed the exchange of O between subsurface and surface that gives rise to the effect shown in Fig. 1. We generated surface V_Os (now by bombarding with electrons from a conventional electron source) and then annealed the surface. It is known that this results in the migration of the surface vacancies to the subsurface region [16]. We then located the subsurface V_Os with STM, and pulled them back to the surface by applying a high sample bias.

Figure 2(a) shows the anatase surface after exposing it to the electron beam. Surface V_Os are marked. The V_O concentration decreases after annealing above 200 K, with no discernible trace in STM images [16]. However, when the annealing temperature exceeds room temperature, new features are observed. Several types formed, with a characteristic and reproducible appearance in STM images. These are marked as C2–C5 in Figs. 2(b)–2(e). After annealing to temperatures slightly above 300 K, we observe mostly the features we call C2 [see Fig. 2(c)] and C3 [Fig. 2(b)]. These two are imaged as distortions of the anatase (101) lattice. They appear as protrusions, slightly shifted in the [$\bar{1}$01] direction from the maxima of the bright rows. After annealing the surface to higher temperatures (≈380–500 K), larger features appear [see C4 and C5 in Figs. 2(b) and 2(d) and also in Ref. [16]]. An example of one feature larger than C5 is shown at the bottom of Fig. 2(e).

The features C2–C5 (as well as larger ones, which are not discussed here) are directly related to the oxygen deficiency in the near-surface region, as judged by the disappearance of surface V_Os. We assume that they originate from clustering of the oxygen vacancies that were originally located on the surface, as discussed below. In the nomenclature C2–C5 the number denotes the order in which the clusters form, i.e., C2 forms at the lowest temperatures (≈320 K) and so forth.

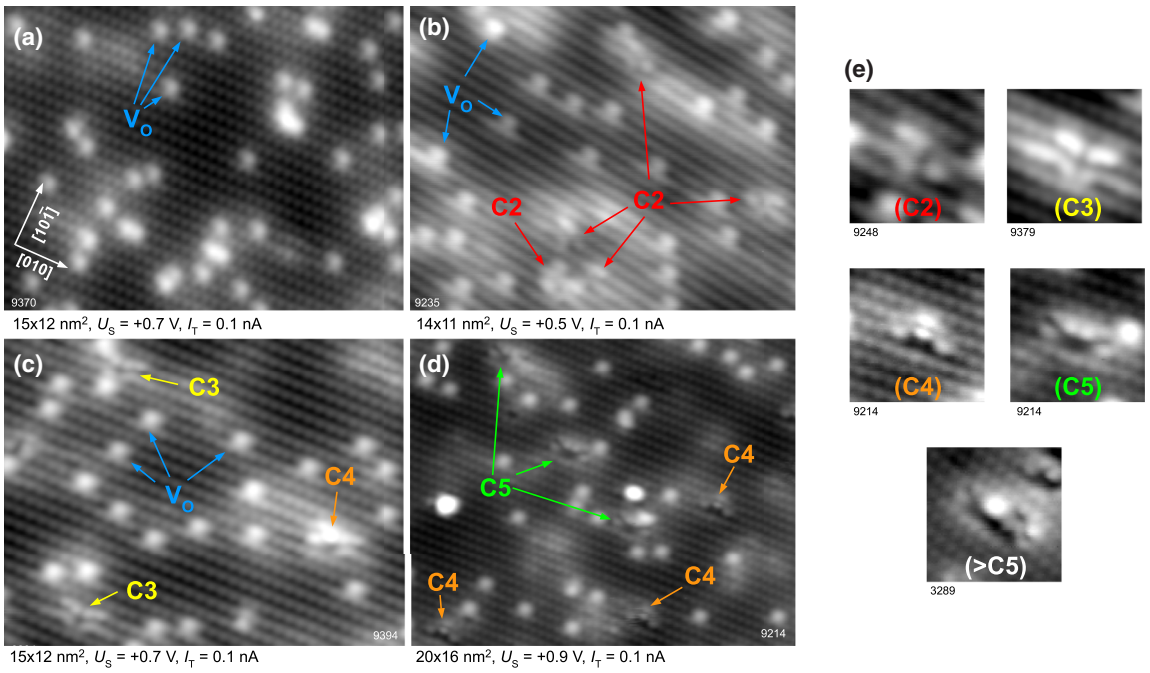

FIG. 2. (Color online) (a) STM image of anatase (101) after exposing the surface to an electron beam at $T = 105$ K (STM image taken at 6 K). Oxygen vacancies (marked V_O) are generated. Electron-bombarded surfaces after annealing for 10 min to (b) 320 K, (c) 340 K, and (d) 380 K. Each panel represents a separate experiment and shows a different area on the sample. Some vacancies migrate to the subsurface and form characteristic V_O clusters, marked as C2–C5. (e) Details of the C2–C5 clusters.

The numbers 2–5 are tentatively related to the number of oxygen vacancies in the cluster. The experiments shown below indicate that C2 contains two vacancies, and C3 three. It is possible that these "clusters" are nucleation centers of more reduced phases of titania, like Ti_2O_3 or TiO.

We note that the activation energy for hopping of a single surface V_O to the first subsurface layer is 0.75 eV according to density functional theory calculations [16,23,24]. A vacancy can possibly migrate deeper with lower activation barriers (as low as 0.17 eV). The energetically most favorable position for a single vacancy is likely in the first few subsurface layers rather than deep in the bulk; the switching between surface and subsurface sites that we observed for sample temperatures 200–300 K in our previous work [16] supports the preferred residence of V_Os in near-surface regions. In order to migrate in the direction parallel to the surface, the vacancy has to perform at least one hop with a calculated activation barrier of $\approx$1.1 eV [24]. The difference in activation energies for vertical vs lateral diffusion is consistent with our observation that the single surface V_Os start to migrate subsurface at temperatures as low as 200 K, but the clusters start to appear above room temperature.

2. *Converting subsurface vacancy clusters into surface vacancies with the STM tip*

The V_O clusters C2–C5 were scanned with a high STM bias. At a positive sample bias voltage of $\approx +5$ eV the clusters are converted into groupings of single V_Os, with each one characteristic for one type of cluster. This is shown in Fig. 3. The panels (a), (c), and (e) on the left show surfaces with various types of V_O clusters. These surfaces were prepared as described above, i.e., by bombarding a clean anatase (101) surface with electrons and subsequent annealing to 320, 340, and 380 K, respectively. The STM images in panels (b), (d), and (f) at the right were taken after each area was scanned at the bias voltages and high tunneling currents indicated in the large arrows in Fig. 3.

The high-bias scans cause the disappearance of the surface distortions that are indicative of the V_O clusters. The original (1×1) surface is obtained and surface V_Os appear, with a number that is characteristic for each cluster. The cluster C3 is always converted into three V_Os that are usually arranged in the triangular pattern shown in Fig. 3(d). Cluster C2 is converted into a pair of oxygen vacancies. Larger clusters (C4 and higher) can rarely be converted into single oxygen vacancies [see Figs. 3(e) and 3(f)], even if higher electric fields are applied. Usually the cluster undergoes certain changes and some surface V_Os appear, but the original (1×1) surface could not be restored. Probably the crystal lattice is too distorted for the larger clusters; in addition, interstitial Ti atoms [25] may already be involved.

The high-bias scans above the clusters were performed both in the constant current and the constant height modes, providing the same result. (We performed this test to ensure that the tip-sample distance is the same above the cluster and the clean surface.) Compared to the sample bias needed to obtain a comparable number of V_Os on a clean surface (the experiment in Fig. 1), the bias for converting subsurface V_O clusters to surface V_Os is only $\approx$0.3 V lower. The similar values indicate that the physical mechanism is the same in both cases: The surface V_Os are not generated by desorbing oxygen atoms from the surface, but by transport of material within the sample.

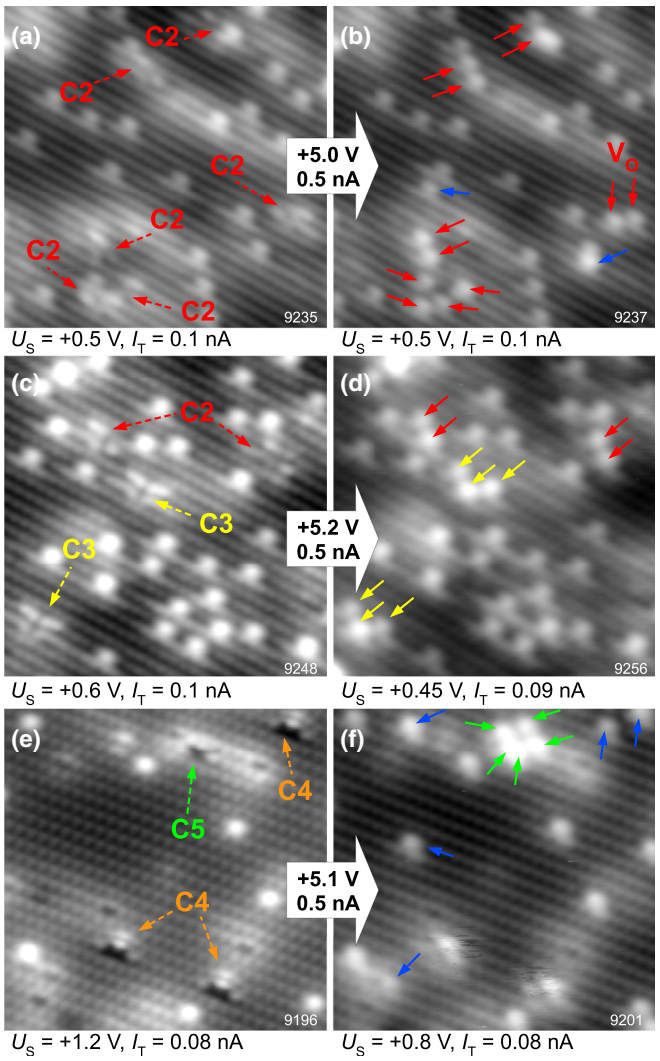

FIG. 3. (Color online) Electronically induced conversion of subsurface vacancy clusters back into single surface V_Os. Pairs of panels (a),(b), and (c),(d), and (e),(f) show the same area before and after a high-bias scan ($V_S \approx +5$ V, $I_T = 0.5$ nA). Dashed arrows in the left images show positions and types of vacancy clusters. Full arrows in the right images point to newly formed surface oxygen vacancies.

We have investigated the electronic structure of the V_O clusters. All the clusters show localized states below the Fermi level, an indication of trapped electrons [26]. As an example, we show empty and filled-state STM images of a C3 cluster in Figs. 4(a) and 4(b), respectively. The filled-state image of the C3 cluster shows one large and two small spots. The surrounding anatase lattice shows negligible local density of states below E_F, as expected [26]. Scanning tunneling spectroscopy measurements of the C3 cluster (data not shown here) show states at ≈ -0.3 (larger spot) and ≈ -0.6 eV (two smaller spots) below the Fermi level. These states appear shallower than the state for a single surface V_O, which is typically -1.0 eV below E_F [26,27].

3. *Impact of the V_O clustering on the materials properties*

Our results clearly show that V_Os tend to form clusters in the subsurface region. In TiO_2 rutile, extended defects form already at V_O concentrations as low as 0.001 [28,29]. No such reports exist for anatase so far, but existence of the V_O clusters in reduced anatase also seems consistent with photoelectron spectroscopy data, where a considerable Ti^{2+} signal was detected in a synchrotron-beam-damaged material [30] (compared to usual Ti^{4+} and Ti^{3+} in rutile) [9]. The V_O clustering must be due to a lower energy as compared to single V_Os. As charged vacancies will repel each other, this indicates that V_O clusters are neutral or carry only a single negative charge per cluster. We note that the vacancy charge state can be possibly influenced by other defects nearby, thus the clustering may be affected by impurities in the material, for example.

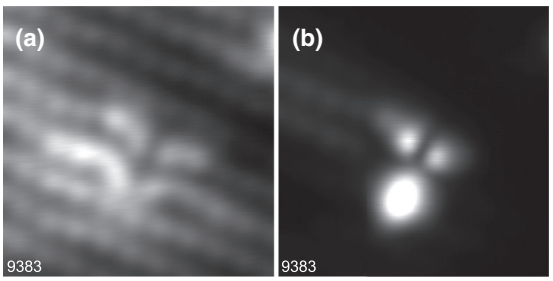

FIG. 4. Empty- and filled-state STM image of a C3 cluster. Constant-height images measured at the same position and the same tip-sample distance. (a) $U_S = +0.5$ V. (b) $U_S = -0.6$ V.

The presence of the V_O clusters needs to be considered in the various applications of this material. For example, single subsurface V_Os are frequently considered in calculations of chemical reactions. In previous studies it was proposed that subsurface V_Os can migrate back to the surface upon adsorption of certain species, and directly participate in chemical reactions [17,31]. It was predicted theoretically that adsorption of an O_2 molecule above a subsurface V_O should result in the migration of the V_O towards the surface and in a bridging interstitial dimer $(O_2)_O$ [17]. However, in the same work it was shown experimentally that this reaction occurs rarely. The number of $(O_2)_O$ features obtained in this way was only on the order of 0.1%–1% ML. A similar reaction was theoretically predicted for H_2O adsorption. Reaction of a H_2O molecule with a subsurface V_O should result in two bridging hydroxyl groups [31]. This reaction has never been observed experimentally, however. Instead it is known that water adsorbs molecularly on the anatase (101) surface [32]. The V_O clustering observed here may explain why it is rare that the vacancies enter the chemical reactions. Theoretical works so far only investigated the configuration of a single subsurface oxygen vacancy. Our results indicate that more favorable configurations exist, where several V_Os are bunched together in a cluster. Breaking such cluster and moving one of its V_Os to the surface is therefore energetically more costly than moving a single V_O from the subsurface region to the surface. The single subsurface V_Os are probably a rare species on the anatase (101) surface compared to, e.g., oxygen vacancies on the rutile (110) surface.

The observed behavior of the V_O clusters is also closely related to memristor research. We have shown that annealing of a reduced anatase surface leads to the clustering of the V_Os. On the other hand, the clusters can be disassembled back into single V_Os under influence of applied electric field

and tunneling current. It is known that the formation of extended defects and reduced Magnéli phases [28,29] and their transformation back into the stoichiometric oxide is a key process in the memristive switching. We have observed the initial step of the V_O aggregation and decomposition. In the following section, we perform a statistical analysis of the experimental data and characterize physical mechanisms responsible for the V_O migration.

C. Physical mechanisms of STM-induced V_O migration

1. Dependence of V_O formation on STM parameters

For simplicity, we focus on single vacancies, i.e., we start each experiment with a clean surface and conduct experiments as the one laid out in Fig. 1. We investigate how the sample bias, tunneling current, and number of scans affect the concentration of V_Os that form during such high-bias scans. Our main findings are summarized in Fig. 5. In Fig. 5(a), we chose a fixed $U_S = +5.6$ V for the high-bias scans and investigated the concentration of V_Os in dependence of the number of scans. This procedure was repeated for different tunneling currents. A new surface area was used for each value of I_T. During all experiments shown in Fig. 5 the size of the scan area and the total scan time were kept constant at 15×15 nm^2 and $\tau = 100$ s, respectively. A similar data set with a lower $U_S = +4.8$ V is shown in Fig. 5(b).

The results in Fig. 5(a) show that the V_O density approaches a saturation value that depends on the tunneling parameters. We then investigated the rate of V_O generation in the zero V_O concentration limit, i.e., the initial slope of the curves in Fig. 5(a). This is depicted in Fig. 5(c) for different combinations of U_S and I_T. Plotted is the V_O concentration obtained after the first two high-bias scans. Within the range of currents investigated here (80–1500 pA) this initial rate is roughly proportional to the tunneling current, a clear indication for a single-electron process. The proportionality is less precise in the data sets measured at higher U_S, as the $n(t)$ curves approach the saturation value faster and the assumption of the zero V_O concentration is not perfectly fulfilled.

To estimate the dependence on the sample bias, the curves in Fig. 5(c) were fitted by a linear function $y = aI_T + b$. The slope a is plotted in the inset of Fig. 5(c). Here the y axis is given in units of cross section $\sigma\,[m^2/C]$, using the known value of the scanned area A and scan time per frame τ. No vacancies are generated below a threshold bias of $U_S = +4.3$ V. From the available data we judge that the dependence follows a polynomial behavior above the threshold, likely quadratic or cubic.

The data shown in Fig. 5 have been measured at a temperature of 78 K. A similar experiment was performed at $T = 6$ K, with a comparable result. This suggests that the V_O migration is not activated thermally.

2. Electric field

The results in Fig. 5 clearly show that a threshold U_S (or perhaps a threshold electric field E) is necessary so that subsurface V_Os move to the surface (or, conversely, surface O are pushed into the lattice) during STM scans. The initial rate of surface/subsurface O exchange is roughly proportional to

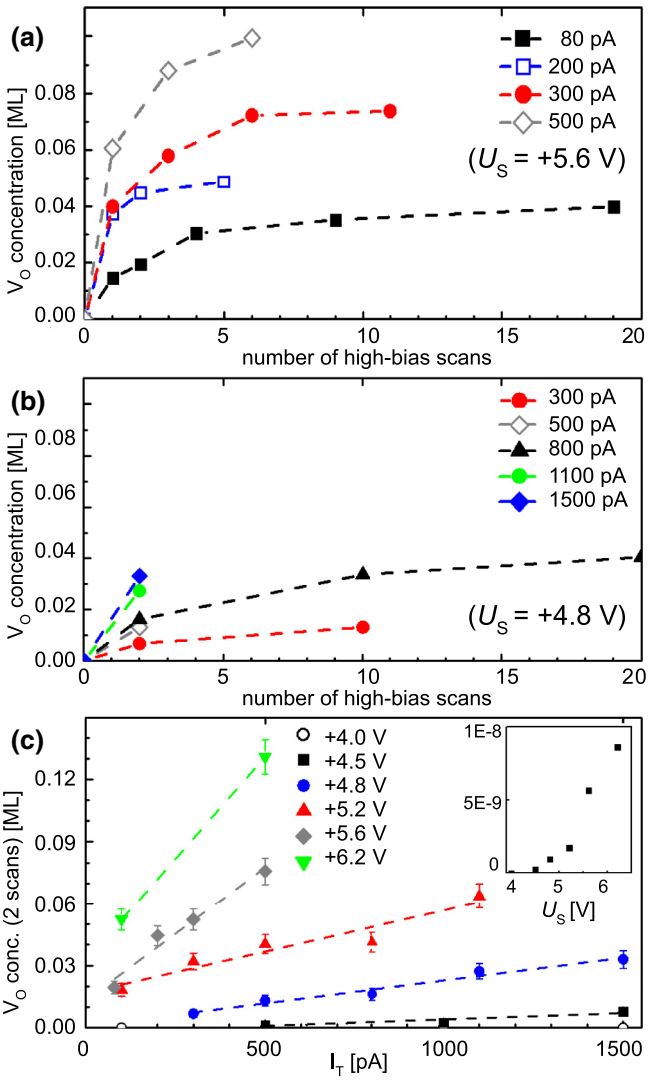

FIG. 5. (Color online) (a) Concentration of V_Os after scanning multiple times at a high STM bias (such as in Fig. 1). Each scan was conducted at $U_S = +5.6$ V and the indicated tunneling currents. (b) The same for a lower $U_S = +4.8$ V. (c) Concentration of V_Os obtained in two high-bias scans, plotted as a function of U_S and I_T. The inset shows the slopes of the curves as a function of U_S. All data obtained at $T = 78$ K with the same STM tip.

I_T, suggesting that a one-electron process is involved. The rate shows a polynomial dependence on U_S above the threshold of +4.3 V. The tip-induced vacancy migration is self-limiting, and the final V_O concentration after many scans also depends on U_S and I_T [Figs. 5(a) and 5(b)].

In tip-induced processes, the tunneling current I_T, bias voltage U_S, and electrical field E inside the sample [33] can all play a role. It is not trivial to disentangle how E depends on the tunneling parameters. The tip-sample distance d depends on U_S and I_T, and only part of the field penetrates into the semiconductor due to screening. This "tip-induced band bending (TIBB)," in turn, can depend on the presence of surface V_Os.

To determine the electric field at the conditions where V_Os appear, we performed local spectroscopy measurements.

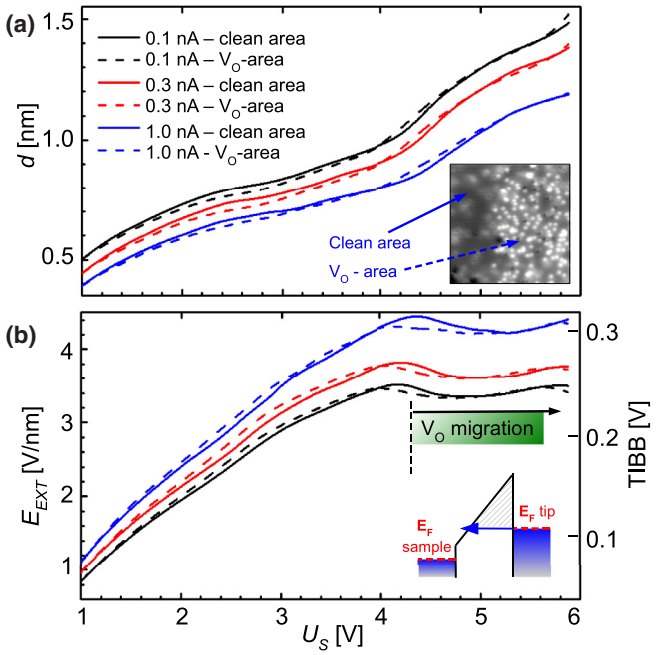

FIG. 6. (Color online) Estimation of the electric field between the tip and the sample. (a) $d(U_S)$ curves measured above the surface with closed feedback loop at different tunneling currents. The curves were measured above the clean surface and in an area with surface V_Os as shown. Measured at $T = 6$ K. d is the absolute tip-sample distance. (b) Calculated electric field between the tip and the sample. The right axis shows an estimate of the TIBB inside the sample. The tunneling scheme in the inset explains why the field only depends on the I_T at higher U_S values (see the text for details).

To avoid high tunneling currents, $z(U_S)$ spectroscopy with a closed feedback loop was used. The measurement time for the curves was set as low as possible (100 ms/curve), in order to avoid additional creation of vacancies during the measurements. The data shown are averages of ten curves measured at different positions. Figure 6(a) shows the result in terms of the absolute tip-sample separation d. We calibrated d by "touching the surface" (see Refs. [26,34]). For $U_S = +1.0$ V and $I_T = 0.1$ nA, we estimate that $d_0 = 0.5$ nm; all other values can be derived by measuring $z(U_S)$ and $z(I)$ spectra.

In Fig. 6(b) we converted the measured $z(U_S)$ curves into the external electric field acting between the tip and the surface. The electric field is approximately $E_{EXT} = U_S/d$. A more precise expression

$$E_{EXT} = \frac{0.94(U_S - U_{LCPD})}{d} \quad (1)$$

takes into account the local contact potential difference between the tip and the sample, U_{LCPD}. We use a value of +0.6 V, assuming work functions of 5.1 and 4.5 eV for the anatase surface and the tip, respectively [35–37]. The factor 0.94 in Eq. (1) is a correction for the TIBB—we estimate that 4%–8% of the applied bias penetrates into the sample. This value was obtained with Feenstra's Poisson equation solver [38], for various combinations of relevant input parameters. This relatively low level of TIBB results from the high dielectric constant of anatase ($\epsilon_r \approx 35$) [33,39], and high sample doping. (Our sample is Nb doped [17] with $n = 10^{20}$–10^{21} cm^{-3}.)

In order to know whether the surface V_Os influence the electric fields acting in the system, we performed $z(U_S)$ measurements in a region where such V_Os had been created with the STM tip (see dashed lines in Fig. 6). The spectra were taken at least two lattice constants away from V_Os (concentration of 7%). There is a small, but reproducible difference in $z(U_S)$ measurements and $E_{EXT}(U_S)$ estimates between clean and defective areas.

The curves in Fig. 6(b) show a plateau above $U_S = +4$ V. This is explained by the tunneling scheme in the inset of Fig. 6(b). When the applied U_S approaches the sample work function, the tunneling barrier (hatched area) only depends on the electric field between the tip and the sample. The field emission regime is almost reached. Interestingly, the onset of this plateau coincides with the threshold for tip-induced vacancy creation, $U_S = +4.3$ V. The electric field is roughly constant in the whole regime of tip-induced vacancy migration [$U_S \geqslant 4.3$ V; inset in Fig. 6(b)]. On the other hand, the rate of V_O migration increases dramatically with U_S in this range. This clearly shows that the voltage dependence is not related to the field. The values of the electric field in the regime of vacancy migration, 3.3–4.5 V/nm [depending on I_T; see Fig. 6(b)] correspond to a TIBB of 0.25–0.30 V inside the sample.

This allows direct comparison of our experimental conditions to the density functional theory calculations performed by Selcuk *et al.* [33]. The calculations show that an electric field inside the anatase sample affects the energetics of surface vs subsurface V_Os. The surface V_O should become $\approx$0.2 eV more favorable at electric fields comparable to our experimental conditions. On the other hand, the field does not reduce the energy barrier for V_O migration from the subsurface to surface, which remains 0.5–0.9 eV. In the following we will argue that hot electrons that are injected from the STM tip into the sample help overcome this activation barrier.

3. *Quantitative analysis*

We have measured data sets similar to the one in Fig. 5(a) for five different values of U_S. All data shown below were obtained with a single STM tip. Here we analyze these results to determine how the V_O concentration scales with the physical quantities E, U_S, I_T, and the time t.

The data are plotted in Fig. 7. The points measured for each single value of U_S collapse to a single line if we scale the axes in a suitable way. Our initial data analysis has shown that the V_O migration is initiated by a single-electron process. Thus an appropriate scale for the x axis is the time multiplied by the current density i. This product is the electron dose per unit area applied during a scan or a sequence of scans; it does not depend on how the tunneling current is distributed under the tip. The y axis shows the V_O concentration n, divided by the electric field ($E - E_0$). We found that this scaling is necessary to collapse the values for different I_T on one line. The value of E for each data point was determined from Fig. 6(b). The scaling used in Fig. 7(a) efficiently separates the effects of I_T and E, as all the data sets obtained for single values of U_S follow lines on a linear-log scale. The parameter E_0 was varied

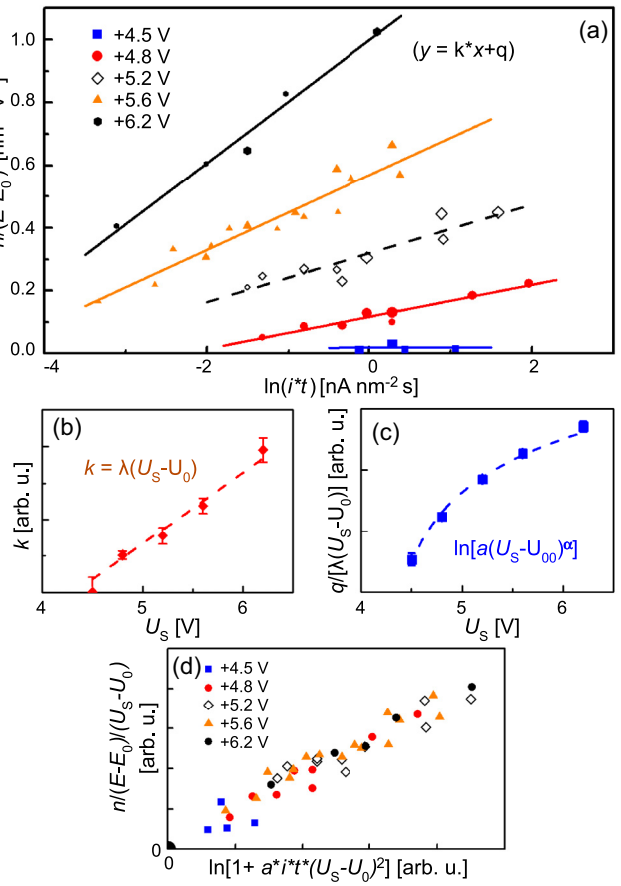

FIG. 7. (Color online) (a) Experimentally measured V_O concentration as a function of the tunneling current I_T (normalized to the scan area, $i = I_T/A$), sample bias U_S, and scanning time t. The size of the data points reflects the tunneling current used (I_T, which ranged from 0.08 to 1.5 nA). See text for scaling of the axes. The data set for each U_S was fitted by a linear function $y = kx + q$. The fitting parameters k and q are further analyzed in (b) and (c) as a function of U_S (see also the Appendix). (d) with a suitable scaling, all experimental data points collapse to a single line.

to maximize the R factors of linear fits in all data, resulting in $E_0 = 2.6 \pm 0.4$ V/nm. We note that scaling the y axis by $(E - E_0)$ is a simple approximation of any E dependence, as the range of E used in our experiments is very small [Fig. 6(b)]. Scaling by E^2 or E^3 provides a very similar result.

The data points in Fig. 7(a) are fitted by linear curves

$$\frac{n}{(E - E_0)} = k \ln(it) + q, \tag{2}$$

where k and q now only depend on U_S. By fitting $k(U_S)$ and $q(U_S)$ by suitable functions [shown in Figs. 7(b) and 7(c)] and inserting these functions into Eq. (2), we arrive at an analytical expression

$$n = \lambda(E - E_0)(U_S - U_0)\ln[a(U_S - U_0)^2 it + 1]. \tag{3}$$

Here $U_0 = 4.3 \pm 0.3$ V and a and λ are constants. [For details of the fitting, including the meaning of parameters displayed in Fig. 7(c) and the origin of the "+1" in Eq. (3), see the Appendix.] Using Eq. (3) we can scale all experimental data points into a single linear dependence [see Fig. 7(d)]. We note that Eq. (3) is the solution of equation

$$\frac{dn}{dt} = ai(U_S - U_0)^3(E - E_0)\exp\left(-\frac{n}{\lambda(E-E_0)(U_S - U_0)}\right), \tag{4}$$

where dn/dt is the vacancy flow towards the surface. In the following we analyze Eq. (4) to gain insight into the physics of the STM-induced vacancy migration.

D. Discussion of possible physical mechanisms

The equation has a form of $dn/dt \approx Re^{-\alpha n}$. Here R is a rate, which is exponentially "damped" by V_Os already present at the surface. R is proportional to the current density i. The term $(U_S - U_0)^3$ has the largest influence on the cross section of the process. The STM bias voltage U_S is the maximum energy of the electrons injected into the sample. A minimum energy (U_0) is needed, and the rate strongly increases with the electron energy above this threshold. In other words, "hot electrons" are needed. One possibility is that the electrons must be injected into a specific electron state in the conduction band to initiate the V_O migration. The importance of injecting the electrons into s orbitals has previously been proposed for tip-induced migration of hydrogen atoms absorbed in bulk palladium [40–42]. While such a process must remain speculative at this point, we note that the experimental value of $U_0 = +4.3$ V matches the region where the d character of the conduction band changes to s-like according to theoretical calculations of the anatase band structure [26,43].

The damping term $\exp\{-n/[\lambda(E - E_0)(U_S - U_0)]\}$ indicates that the efficiency of the electronic excitations decreases with growing surface V_O concentration. The influence of the V_Os already present on the surface can be suppressed by applying a higher electric field and a higher U_S. The first term could be due to surface V_Os screening the field penetrating into the sample. This decreases the TIBB, which is a necessary component of the V_O migration process. The dependence on U_S may be related to scattering the hot electrons at the surface V_Os. Each V_O provides two localized electrons with a state $\approx$1 eV deep in the band gap. The electrons injected from the tip can possibly excite the V_O electrons to the conduction band, resulting in a significant energy loss of the primary electron. The $(U_S - U_0)$ term in the exponential would be then related to the cross section of this electron-electron scattering process.

A brief summary of the role of U_S and I_T is as follows: U_S determines the energy of electrons injected into the material. This in turn determines to which particular energy band in the conduction band they are injected and the energy available for single-electron processes. The tunneling current influences the process in two ways. First, it determines the rate of electronic excitations (rate R is a linear function of I_T). Second, I_T is linked to the electric field acting in the system (see Fig. 6). We note that for constant-current conditions, the electric field does not change significantly with U_S in the regime used for inducing the V_O migration.

Our finding that hot electrons play a role in the V_O migration is in agreement with memristor research. In Ref. [3] it is argued that simple Joule heating may not be the only mechanism involved in defect migration within the crystal. Hot electrons may be directly scattered at defects in the oxide lattice, providing energy for material transport. Our experiments also

show that the electric field layout inside the sample plays a certain role. The field helps to revert the energy balance in the material, providing a direction for the vacancy flow. The value of the electric field varies only slightly under our experimental conditions, therefore the field dependence could not be exactly characterized and was only approximated by a linear function in the equations.

IV. CONCLUSIONS

We have shown that scanning the anatase (101) surface at high positive sample bias results in the appearance of surface V_Os in the scanned area. We attribute this effect to a migration of V_Os from the subsurface region to the surface. The process is self-limiting: the presence of V_Os on the surface prevents further subsurface-to-surface V_O migration. Analysis of the experimental data indicates that the electric field penetrating into the sample is an important factor for reverting the energy balance between the surface and subsurface V_Os. The hot electrons injected from the tip provide the activation energy necessary for the V_O migration through the lattice.

It was further shown that V_Os can easily form subsurface clusters upon annealing. We identified V_O clusters that contain two to five vacancies. Likely this is the initial step in the formation of extended defects and reduced TiO_{2-x} phases. Subsurface aggregates of V_Os can be converted back into single surface V_Os by applying a suitable electric field. This process closely resembles memristive switching: Two distinct states exist, one that is reached upon thermal annealing and another one by applying a high electric field. The memristive behavior of oxides has been investigated for more than 50 years, yet there is essentially no knowledge about processes occurring at atomic scale. Our results could provide a significant step forward to identifying the underlying physical mechanisms.

ACKNOWLEDGMENTS

This work was supported by the ERC Advanced Research Grant "OxideSurfaces," and by the Austrian Science Foundation (FWF) under Funktionelle Oxidoberflächen und Oxidgrenzflächen (FOXSI) Project No. F45.

APPENDIX: FITTING DETAILS

Fitting the data points in Fig. 7(a) by $y = kx + q$ provides dependencies $k(U_S)$ and $q(U_S)$ displayed in Figs. 7(b) and 7(c), respectively. The $k(U_S)$ appears linear, $k = \lambda(U_S - U_0)$, with $U_0 = 4.3 \pm 0.4$ V and $\lambda = 0.10 \pm 0.01$ V^{-2} nm^{-1}. One can rewrite Eq. (2) as

$$\frac{n}{\lambda(E - E_0)(U_S - U_0)} = \ln(it) + \frac{q}{\lambda(U_S - U_0)}. \quad \text{(A1)}$$

We can fit the quantity $q/[\lambda(U_S - U_0)]$ as a function of U_S [see Fig. 7(c)]. A suitable function is logarithmic; we use an ansatz of $\ln[a(U_S - U_{00})^\alpha]$. Based on the initial analysis in Fig. 5 we guess an α close to 2, and U_{00} similar to U_0. Fitting the plot in Fig. 7(c) indeed provides $\alpha = 2.2 \pm 0.5$, $U_{00} = 4.2 \pm 0.2$ V, and $a = 40 \pm 20$ A^{-1} s^{-1} $V^{-\alpha}$. We will further consider $U_{00} \equiv U_0$ and $\alpha = 2$. The relation for n can be expressed as

$$n = \lambda(E - E_0)(U_S - U_0)\ln[a(U_S - U_0)^2 it]. \quad \text{(A2)}$$

The disadvantage of this equation is its divergence at $t = 0$. By taking the derivative of Eq. (A2), we obtain the differential equation, Eq. (4). By solving this equation, we obtain an integration constant: "+1" in the logarithm [see Eq. (3)]. This ensures the initial condition $n = 0$ at $t = 0$. With the integration constant known, we repeated all the fittings in Fig. 7(a). It turns out that the impact on all values obtained from the fitting is very small, as the "+1" term in the logarithm is negligible for most data points. The only fitting constant that is affected significantly is a. The new value of $a = 10$ A^{-1} s^{-1} $V^{-\alpha}$ was used in Fig. 7(d).

We note that the fitting presented in this paper leads to the final equation (4) in the form $dn/dt \approx Re^{-n}$. We have tried other ways of fitting the data, especially those leading to the Langmuir-type behavior $dn/dt \approx R(1 - \theta)$. The experimental data do not fit such a behavior well.

[1] D. B. Strukov, G. S. Snider, D. R. Stewart, and R. S. Williams, Nature (London) **453**, 80 (2008).
[2] J. J. Yang, D. B. Strukov, and D. R. Stewart, Nat. Nanotechnol. **8**, 13 (2013).
[3] K. Szot, G. Bihlmayer, and W. Speier, *Solid State Physics*, Chap. 4, Vol. 65 (Elsevier, Amsterdam, 2014), pp. 353–544.
[4] K. Szot, M. Rogala, W. Speier, Z. Klusek, A. Beshmen, and R. Waser, Nanotechnology **22**, 254001 (2011).
[5] H. Zheng, J. Kröger, and R. Berndt, Phys. Rev. Lett. **108**, 076801 (2012).
[6] H. Zheng, A. Weismann, and R. Berndt, Phys. Rev. Lett. **110**, 226101 (2013).
[7] N. Q. Minh, J. Am. Ceram. Soc. **76**, 563 (1993).
[8] B. C. H. Steele and A. Heinzel, Nature (London) **414**, 345 (2001).
[9] U. Diebold, Surf. Sci. Rep. **48**, 53 (2003).
[10] Z. Dohnálek, I. Liubinetsky, and R. Rousseau, Prog. Surf. Sci. **85**, 161 (2010).
[11] A. Linsebigler, G. Lu, and J. Yates, Chem. Rev. **95**, 735 (1995).
[12] M. A. Henderson, Surf. Sci. Rep. **66**, 185 (2011).
[13] M. Grätzel, Nature (London) **414**, 338 (2001).
[14] Y. Furubayashi, T. Hitosugi, Y. Yamamoto, K. Inaba, G. Inoda, Y. Hirose, T. Shimada, and T. Hasegawa, Appl. Phys. Lett. **86**, 252101 (2005).
[15] Y. He, O. Dulub, H. Z. Cheng, A. Selloni, and U. Diebold, Phys. Rev. Lett. **102**, 106105 (2009).
[16] P. Scheiber, M. Fidler, O. Dulub, M. Schmid, U. Diebold, W. Hou, U. Aschauer, and A. Selloni, Phys. Rev. Lett. **109**, 136103 (2012).
[17] M. Setvín, U. Aschauer, P. Scheiber, Y.-F. Li, W. Hou, M. Schmid, A. Selloni, and U. Diebold, Science **341**, 988 (2013).
[18] O. Dulub and U. Diebold, J. Phys.: Condens. Matter **22**, 084014 (2010).
[19] M. Setvin, B. Daniel, V. Mansfeldova, L. Kavan, P. Scheiber, M. Fidler, M. Schmid, and U. Diebold, Surf. Sci. **626**, 61 (2014).
[20] P. Ebert, Surf. Sci. Rep. **33**, 121 (1999).

[21] O. Dulub, M. Batzil, S. Solovev, E. Loginova, A. Alchagirov, T. E. Madey, and U. Diebold, Science **317**, 1052 (2007).
[22] X. Cui, B. Wang, Z. Wang, T. Huang, Y. Zhao, J. Yang, and J. G. Hou, J. Chem. Phys. **129**, 044703 (2008).
[23] H. Cheng and A. Selloni, Phys. Rev. B **79**, 092101 (2009).
[24] H. Cheng and A. Selloni, J. Chem. Phys. **131**, 054703 (2009).
[25] S. Wendt, P. T. Sprunger, E. Lira *et al.*, Science **320**, 1755 (2008).
[26] M. Setvin, C. Franchini, X. Hao, M. Schmid, A. Janotti, M. Kaltak, C. G. Van de Walle, G. Kresse, and U. Diebold, Phys. Rev. Lett. **113**, 086402 (2014).
[27] M. Setvin, X. Hao, B. Daniel, J. Pavelec, Z. Novotny, G. S. Parkinson, M. Schmid, G. Kresse, C. Franchini, and U. Diebold, Angew. Chem., Int. Ed. **53**, 4714 (2014).
[28] L. A. Bursill and D. J. Smith, Nature (London) **309**, 319 (1984).
[29] L. A. Bursill and M. G. Blanchin, J. Solid State Chem. **51**, 321 (1984).
[30] M. Jackman, A. G. Thomas, P. Deak, K. L. Syres *et al.*, arXiv:1406.3385.
[31] Y. Li and Y. Gao, Phys. Rev. Lett. **112**, 206101 (2014).
[32] U. Aschauer, Y. He, H. Cheng, S.-C. Li, U. Diebold, and A. Selloni, J. Phys. Chem. C **114**, 1278 (2010).
[33] S. Selcuk and A. Selloni, J. Chem. Phys. **141**, 084705 (2014).
[34] P. Jelinek, M. Svec, P. Pou, R. Perez, and V. Chab, Phys. Rev. Lett. **101**, 176101 (2008).
[35] G. Xiang, R. Shao, T. C. Droubay, A. G. Joly, K. M. Beck, S. A. Chambers, and W. P. Hess, Adv. Funct. Mater. **17**, 2133 (2007).
[36] D. O. Scanlon, C. W. Dunnil, J. Buckeridge, S. A. Shevlin *et al.*, Nat. Mater. **12**, 798 (2013).
[37] S. Loth, Ph.D. thesis, Universität Göttingen, 2008.
[38] R. M. Feenstra, S. Gaan, G. Meyer, and K. H. Rieder, Phys. Rev. B **71**, 125316 (2005).
[39] R. J. Gonzalez, R. Zallen, and H. Berger, Phys. Rev. B **55**, 7014 (1997).
[40] M. Blanco-Rey, M. Alducin, J. I. Juaristi, and P. L. de Andres, Phys. Rev. Lett. **108**, 115902 (2012).
[41] E. C. H. Sykes, L. C. Fernandez-Torres, S. U. Nanayakkara, B. A. Mantooth, R. M. Nevin, and P. S. Weiss, Proc. Natl. Acad. Sci. USA **102**, 17907 (2005).
[42] T. Mitsui, E. Fomin, D. F. Ogletree, M. Salmeron, A. U. Nilekar, and M. Mavrikakis, Angew. Chem., Int. Ed. **46**, 5757 (2007).
[43] M. Landmann, E. Rauls, and W. G. Schmidt, J. Phys.: Condens. Matter **24**, 195503 (2012).